Near Ultra-Violet absorbers for transparent organic solar cells

Chaima Mahmoudi, Wenziz Muzuzu, Sadiara Fall, Yuhan Zhong, Christophe Melart, Patrick Lévêque, Thomas Heiser, Nejmeddine Smida Jaballah, Mustapha Majdoub, Nicolas Leclerc

Near Ultra-Violet absorbers for transparent organic solar cells

C. Mahmoudi,[a,b] W. Muzuzu,[b] S. Fall,[c,*] Y. Zhong,[c] C. Mélart,[b] P. Lévêque,[c] T. Heiser,[c] N. S. Jaballah,[a] M. Majdoub,[a] N. Leclerc[b,*]

[a] Laboratoire des Interfaces et Matériaux Avancés (LIMA), Faculté des Sciences de Monastir (Université de Monastir), Bd. De l'Environnement, 5019 Monastir, Tunisia.

[b] Institut de Chimie et Procédés pour l'Énergie, l'Environnement et la Santé (ICPEES), UMR 7515-CNRS, Université de Strasbourg, ECPM, 25 rue Becquerel, 67087 Strasbourg, France. *E-mail: leclercn@unistra.fr

[c] Laboratoire ICube, UMR 7357-CNRS, Université de Strasbourg, 23 rue du Loess, 67037 Strasbourg, France. *E-mail: sadiara.fall@unistra.fr

Abstract

We describe the synthesis of two new dumbbell-shaped small molecules used as near ultra-violet absorbers for transparent organic solar cell application. The electron-donor TAT units, sandwiching the central chromophore, constitute very efficient π-stacking platforms that are nevertheless highly soluble thanks to the presence of three alkyl chains. The TAT units are used in combination, with a small central electron donor unit, either a carbazole or a thieno[3,2-*b*]thiophene (TT) unit. The two new dumbbell-shaped small molecules including only electron-donor units are strongly absorbing in the near UV range, due to the reduced electronic conjugation. Combined with a suitable hole mobility, the most conjugated thieno[3,2-*b*]thiophene-based derivative, when used as electron-donor component in a bulk heterojunction organic solar cell, exhibits a 48% of average visible transmittance with a power conversion efficiency close to 2%.

Keywords: Transparent organic solar cells, Near Ultra-Violet organic dyes, wide bandgap organic materials.

1. Introduction

Transparent solar cells (TSCs) are essential for the development of photovoltaic glazing to be integrated in buildings and automotive vehicles.[1-3] However, transparent photovoltaic devices are difficult to obtain with inorganic semiconductor materials, which are opaque by nature, due to the thickness of the material required and the difficulty of modulating their absorption wavelength range.[4] Such TSCs, involving wide bandgap inorganic materials, are currently limited to a few percent of power conversion efficiencies (PCE) with average visible transmittance (AVT) of maximum 40-50%.[5] In this context, organic semiconducting materials appear as highly appealing candidates towards semi-transparent or fully transparent PV devices. A first route towards transparency is to use them as ultra thin films. The corresponding active layers allow for semi-transparent devices regardless of the absorption range of the materials selected.[6] Indeed, significant research efforts have been devoted to adjust the active layer thickness to find a trade-off between photon harvesting and charge generation.[7] For instance, Zhang *et al*. reported recently a highly efficient semi-transparent solar cell by optimizing the thickness of the active layer of the reference binary blend, PM6:Y6.[8] They succeeded to reach a PCE as high as 12.4% with an AVT of more than 18%. A second strategy consists in designing new transparent organic semiconductors, which include either near-ultra-violet (NUV) or near infra-red (NIR) absorbers. The latter have become the most common with the emergence of non-fullerene NIR absorbing acceptors (NFAs). Thus, the most common strategy of

using NIR absorbers for TSCs, consists in using donor and acceptor components exhibiting a strong overlap of their absorption profiles in the NIR region, resulting in transparency in the visible region. Consequently, an AVT higher than 50% has been reached with PCEs in the 4-5% range. A key feature of this approach is the diversity of possible chemical structures, both for the electron donor and the electron acceptor. As an example, Y. Sun and coworkers have recently developed TSCs, using a simple alternated D-A copolymer (PDTP-DFBT) as an electron donor with a low bandgap NFA (FOIC). They achieved efficiencies of 4.2 % for an AVT of 52%.[9] By optimizing the top electrode, they even succeeded to reach AVT of 61% at the cost of a limited PCE decrease (3.5 %). More impressively, R. Durrant *et al.*, also using an electron donor polymer blended with a molecular NFA (DPP2T and IEICO-4F, respectively), measured a PCE of 5.7% with an AVT reaching 61%.[7]

The use of NUV absorbers is much less studied, mainly because by neglecting a large part of the spectral irradiation (wavelengths above 400nm approximately), fewer charge carriers can be generated. However, several publications reporting promising results using NUV absorbers are worth mentioning. Thus, in 2017, Y.L. Loo *et al*. investigated planar bilayer TSC devices processed by thermal evaporation of wide bandgaps small molecules. They reached impressive transparency in the visible range exceeding 80% for PCEs of around 1.3-1.5%.[10] A distinctive feature of solar cells using NUV absorbers is the possibility of obtaining very high photovoltages, due to the wide bandgap materials and in particular to the electron donor components with deep HOMO levels. As an illustration, K. Vandewal *et al.* reported in 2019 an open-circuit voltages (Voc) higher than 2.1 V using a couple of high bandgap molecules deposited by thermal evaporation.[11] Using the same materials, D. Spoltore *et al*. reported recently a PCE of 0.2% with an AVT of 60% and a Voc of about 2V. By using a sexithiophene as electron donor molecule, they reached approximately 1.7% of PCE with an AVT of 50% (Voc ≈ 1.5 V).[12] However, most current NUV-based TSC devices have been produced by thermal evaporation, a costly and non-trivial process for the production of large area devices. Therefore, there is a significant interest to investigate solution-processable NUV blends for TSC devices.

We have recently reported an innovative design of planar dumbbell-shaped molecular electron donors for organic photovoltaic (OPV) devices based on two triazatruxene (TAT) end-groups, sandwiching a π-conjugated central chromophore (see scheme 1). The TAT unit has been introduced as a very efficient π-stacking platform that is nevertheless highly soluble thanks to the presence of three alkyl chains.[13] This electron-donor design allowed partial decoupling of structural, electrochemical and optical properties. Indeed, the structural and charge-transport properties are essentially determined by the general molecular architecture, while the optical band-gap and the frontier molecular orbital energy levels are mainly governed by the selected central chromophore.[14] Recent studies have shown that the alkyl side-chains carried by the TAT units are key-molecular parameters governing the stacking ability of these molecules resulting, under specific conditions, to very unusual and innovative bridge columnar phases.[15,16] In combination with usual electron acceptor fullerene derivatives, these small molecules allow reaching reasonable PCEs.[17] Interestingly, regardless of the central chromophore, this design preserves high Voc, due to the deep HOMO level resulting from the use of TAT units.[18]

Herein, we propose to tune this dumbbell shaped design in order to elaborate NUV absorbers for TSC applications. As stated in the previous paragraph, the central chromophore is a key parameter governing the optical properties. Considering the TAT unit as an electron donor unit, the use of an electron withdrawing central group give rise to an internal charge transfer (ICT) optical transition characterized by an absorption band within the visible wavelength range. Therefore, to avoid this ICT band and enhance transparency in the visible, we replaced the central electron withdrawing group by an electron donating unit. It is expected that the resulting D-D'-D molecular architecture exhibits a wide bandgap with a NUV absorption.

To establish a first set of materials, two elementary chemical units have been selected: an alkyl-free thieno[3,2-*b*]thiophene (TT) and a carbazole unit, carrying a ramified side chain and connected to the TAT units through the most delocalized 2- and 7-positions (Scheme 1). Both units are planar. However, the naked and sterically lightly hindered TT unit is expected to lead to the most conjugated

dumbbell shaped small molecule, while the carbazole-based molecules are expected to be more soluble, easier to process, and even more transparent in the visible range. After a characterization of their optoelectronic properties, these two new small molecules have been used to develop TSC devices that selectively harvest NUV photons. Interestingly, an appealing combination of reasonably high PCE and AVT of 1.8% and 48%, respectively, has been reached when using the new **TAT-TT** molecule blended with the $PC_{71}BM$ fullerene derivative as electron acceptor component. Density functional theory (DFT) and time-dependent DFT (TD-DFT) were used to analyze the experimental results.

2. Materials and methods

2.1. Measurements and characterization

NMR analysis. ^{1}H NMR (400 MHz) and ^{13}C NMR (100 MHz) spectra were recorded at room temperature and at high temperatures (90°C) on a Bruker Advance III HD 400 MHz spectrometer.

UV-Visible Spectroscopy. Absorption spectra in solution and in thin films were recorded on a Shimadzu UV-2600 spectrophotometer. In solid state, the absorption spectra were measured on thin films drop-casted on glass substrates from a 0.5 mg/mL chloroform solution of organic dyes.

Electrochemical measurements. Cyclic voltammetry (CV) was recorded with a VSP BioLogic potentiostat/galvanostat with a scan rate of 100 mV/s using 0.1 M tetrabutylammonium tetrafluoroborate (Bu_4NBF_4) in CH_2Cl_2 as supporting electrolyte, a Ag/AgCl electrode as the reference electrode, a Pt wire electrode as working electrode, a Pt wire as counter electrode and ferrocene/ferrocenium (Fc/Fc+) as a reference. The cell was briefly deoxygenated with argon before each scan.

Thermogravimetric analysis. TGA measurements were carried out on a SDTQ 600 apparatus at scanning rate of 10 °C/min. A differential thermal analysis (DTA) signal was simultaneously measured.

Differential Scanning Calorimetry. DSC measurements were carried out with TA Instruments Q1000 instrument, operated at scan rate of 5°C/min on heating and on cooling.

Computational methods. All calculations of the compounds were performed using the Gaussian 09 software package [19] and Gauss View 5.0 molecular visualization program Package. The theoretical simulations were carried out using density functional theory (DFT) with CAM-B3LYP (Coulomb Attenuated Method-Becke three-parameter Lee–Yang–Parr) exchange-correlation functional.[20] 6-31G(d,p) was used as a basis set for all atoms (C, N, H, O). Therefore, in this work, dependent theory TD-DFT method has been used to simulate the electronic absorption spectra and the orbitals molecular. It is important to consider the solvent effect on theoretical calculations when seeking to predict the experimental spectra with a reasonable accuracy. The oscillator strengths and excited state energies were investigated using TD-DFT calculations on the fully DFT optimized geometries.

Organic Field Effect Transistors. Bottom contact bottom gate OFET structures were fabricated using commercially available silicon substrates. Lithographically defined Au (30 nm)/ITO (10 nm) bilayers were used as source and drain electrodes and 230 nm thick SiO_2 layer as a gate dielectric. Channel length and width were L = 20 µm and W = 10 mm, respectively. Substrates were cleaned consecutively in ultrasonic baths at 45°C for 15 min each step using soapsuds, acetone, and isopropanol and followed by 15 min UV-ozone treatment. Then substrates were transferred into a nitrogen filled glove box where hexamethyldisilazane (HMDS) was spincoated on top of the SiO_2 followed by annealing at 135°C for 10 min. Finally, solutions of pure TAT-based dyes were spincoated substrates to complete the FET devices. For each molecule, a concentration of 4 mg/mL in $CHCl_3$ was used. Prior to characterization, completed devices were dried under high vacuum (≈10^{-5}-10^{-6} mbar).

Transistor output and transfer characteristics were measured using a Keithley 4200 semiconductor characterization system. Hole mobilities were extracted in the saturation regime using a standard device model.

Organic Photovoltaic devices. ITO coated glass substrates were cleaned in ultrasonic soap bath, deionized water, acetone and 2-propanol at 45°C for 15 minutes for each step. Then, they were dried by nitrogen and were treated in a UV/Ozone oven to remove residual organic contaminants. PEIE layer (≈ 7 nm) was spin-coated onto pre-cleaned ITO and thermally annealed at 100°C for 10 min and used as an electron extracting contact. The photoactive layer was prepared from different solutions containing TAT-TT:$PC_{71}BM$ blends and TAT-CBz:$PC_{71}BM$ with a TAT-based dye concentration of 5 mg/ml in $CHCl_3$. The ratio of donor and acceptor was varied from 1:1 to 1:3 in order to find optimal conditions. The solution were spin-coated onto the PEIE/ITO substrates. regarding the TAT-TT:$PC_{71}BM$ blend, an optimal condition has been found after a thermal annealing step at 130°C for 10 min under a nitrogen atmosphere. A 7 nm thick MoO_3 and 120 nm thick Ag layers were thermally evaporated (Pressure ≈ $1x10^{-6}$ mbar) on top the films to complete the solar cell. The effective area of each cell was 12 mm^2.

OPV measurements. The (J-V) curves of the OPV devices were measured under AM 1.5G-100 mW/cm^2 simulated sunlight irradiation. (J-V) characteristic measurements of photovoltaic devices were conducted using LabView-controlled Keithley 2400 SMU. The performance of solar cells under the dark and illumination were measured using a BET Technologies Sun 3000 solar simulator with an AM1.5G filter. All the photovoltaic parameters of solar devices (V_{OC}, J_{SC}, *FF* and *PCE*) were extracted using the LabView software.

2.2. Synthesis

All reagents and chemicals were purchased from commercial sources and used without further purification. The TAT-Br co-monomer was prepared according to the respective reference.[17]

2.2.1. 2,5-bis(trimethylstannyl)thieno[3,2-b]thiophene (TT)

Under an argon atmosphere, 2,5-dibromothieno[3,2-*b*]thiophene (1 eq) was dissolved in dry THF (0.15 M) and cooled to -78°C. In another flask, under argon, diisopropylamine (1.1 eq) was solubilized in dry THF (1.9 M) and cooled to -78°C. Then *n*BuLi (2.2 eq, 2.5 M in hexane) was added dropwise and the solution was kept at -78 °C for 10 min, warm-up 10 min at -20°C, and then cooled down again at -78°C. The lithium diisopropylamide so synthesized, was added slowly to the solution keeping the temperature below -60°C. The cooling bath was removed, allowing the temperature to reach 0°C (ice bath). The solution was then cooled back to -78°C before the addition of trimethyltin chloride (2.2 eq, 1 M in THF). The mixture was stirred over 24 h and allowed to reach room temperature. The mixture was extracted with diethyl ether and the organic phase was washed with water and dried over Na_2SO_4. The solvent was removed under reduced pressure and was further dried under a high vacuum providing the desired compound as a white solid (Yield = 67%).

^{1}H NMR ($CDCl_3$, 400MHz) δ(ppm)= 7.28 (2H, s), 0.42 (18H, t, J=7.8Hz). ^{13}C NMR ($CDCl_3$, 100MHz) δ(ppm)= 147.58, 141.14, 127.32, 126.14, 119.28, 8.34.

2.2.2. 9-(heptadecan-9-yl)-2,7-bis(4,4,5,5-tetramethyl-1,3,2-dioxaborolan-2-yl)-9H-carbazole (Cbz)

The 2,7-dibromo-9-(heptadecan-9-yl)-9H-carbazole (Cbz-Br_2) (1 eq), potassium acetate (6 eq) and Pd(dppf) $2Cl_2.CH_2Cl_2$ (0.2 eq) was added into 1,4-dioxane (0.2 M) and the solution was degassed for 45 minutes. Then 4,4,4',4',5,5,5',5'-octamethyl-2,2'-bi(1,3,2-dioxaborolane) (4 eq) was added and the mixture was heated at 100°C for 24 hours. The solution was quenched with water and extracted with

CH_2Cl_2, washed with water and the organic was dried on Na_2SO_4. After evaporation of the solvent the crude was recrystallized in MeOH to give the desired compound as white crystals (Yield= 80%).

^{1}H NMR ($CDCl_3$, 400 MHz) δ(ppm)= 8.03 (2H, t, J= 8.7 Hz), 7.87 (2H, d, J= 7.6 Hz), 7.57 (2H, d, J= 7.6 Hz), 4.70 – 4.51 (1H, m), 2.25 (2H, ddd, J= 19.6, 11.9, 7.0 Hz), 1.86 (2H, ddd, J= 15.4, 10.1, 4.9 Hz), 1.31 (24H, s), 1.20 – 0.84 (28H, m), 0.73 (6H, t, J= 7.0 Hz). ^{13}C NMR ($CDCl_3$, 100 MHz) δ(ppm)= 152.2, 126.8, 125.7, 125.1, 124.8, 124.64, 115.6, 83.69, 77.32, 77.21, 77.01, 76.69, 56.36, 33.82, 31.76, 29.47, 29.31, 29.20, 26.77, 24.94, 22.59, 14.05.

2.2.3. TAT-TT

The TAT-Br (2eq) and 2,5-bis(trimethylstannyl)thieno[3,2-*b*]thiophene (1 eq) were dissolved in dry toluene in flame dried Schlenk. Then the solution was degassed for 30 minutes and $Pd_2(dba)_3$ (0.02 eq) and P(*o*-tolyl)$_3$ (0.08 eq) were added and the reaction mixture was stirred at 110°C under argon atmosphere for 24 hours. The organic layer was extracted chloroform and washed several times with distilled water and dried over anhydrous sodium sulfate Na_2SO_4. The obtained solution was then concentrated under reduced pressure. Purification was realized by silica gel column chromatography (Silica:Toluene/DCM/Cyclohexane (5/20/75)) following by a precipitation from a DCM/methanol mixture. The pure compound was then filtered and dried under reduced pressure overnight to give a slightly yellow solid (Yield = 40 %).

^{1}H NMR ($CDCl_3$, 400 MHz) δ(ppm)= 8.31 (2H, m), 8.12-8.22 (3H, m), 7.758 (1H, s), 7.534-7.554 (4H, m), 7.361-7.40 (2H, m), 4.81-4.88 (6H, m), 1.919 (6H, m), 1.82 (18H, m), 0.755 (9H, m). ^{13}C NMR ($CDCl_3$, 100MHz): 172.71, 148.41, 138.35, 136.63, 128.81, 125.68, 124.28, 115.08, 114.90, 114.64, 111.78, 110.93, 110.47, 109.99, 108.88, 108.15, 106.15, 98.43, 96.51, 95.40, 48.15, 31.67, 30.78, 27.66, 22.41, 14.03. Anal. Calcd for $C_{90}H_{102}N_6S_2$: C, 81.16; H, 7.72; N, 6.31 Found: C, 81.06; H, 7.69; N, 6.27.

2.2.4. TAT-Cbz

The TAT-Br (2 eq) and 9-(heptadecan-9-yl)-2,7-bis(4,4,5,5-tetramethyl-1,3,2-dioxaborolan-2-yl)-9H-carbazole (1eq) were dissolved in dry toluene in flame dried Schlenk. and a solution of K_2CO_3 (8 eq) in H_2O was added. Then, the solution was degassed for 1 hour and $Pd_2(dba)_3$ (0.02 eq) and P(o-tolyl)$_3$ (0.08 eq) were added and the reaction mixture was stirred at 110°C under argon atmosphere for 48 hours. The organic layer was extracted chloroform and washed several times with distilled water and dried over anhydrous sodium sulfate Na_2SO_4. The obtained solution was then concentrated under vacuum. Purification was carried out by column chromatography (silica gel, Toluene/DCM/ Cyclohexane (5/10/85)). The eluent was concentrated to yield a very pale-yellow solid (Yield = 75 %).
^{1}H NMR ($CDCl_3$, 400 MHz) δ(ppm)= 8.44 (1H, d, J= 8.4Hz), 8.29-8.40 (3H, dt, J=11.8, 7.9), 8.02 (1H, d, J= 14.2Hz), 7.72 -7.90 (3H, m), 7.661-7.23 (2H, dd, J=8.0, 4.4Hz), 7.51 (2H, t, J=7.6Hz), 7.399 (2H, m), 5.127-4.955 (6H, m), 4.894-4.794 (1H, ddd, J=21.3, 14.7, 7.8 Hz), 2.214-1.996 (6H, m), 1.493-1.126 (32H, m), 0.977-0.767 (15H, m). ^{13}C NMR ($CDCl_3$, 100MHz) δ(ppm)= 155.35, 142.78, 138.76, 135.35, 126.23, 125.48, 124.28, 124.18, 123.08, 115.08, 114.98, 114.64, 113.60, 113.21, 113.04, 110.30, 96.92, 96.43, 95.89, 56.36, 48.39, 33.82, 32.18, 31.81, 30.78, 29.48, 29.31, 29.20, 26.77, 28.44, 24.94, 22.59, 14.09, 14.07, 14.03, 13.82. Anal. Calcd for $C_{112}H_{141}N_7$: C, 84.96; H, 8.90; N, 6.14 Found: C, 84.89; H, 8.95; N, 6.08.

3. Results and discussion

3.1. Synthesis and structural characterization

The synthesis routes of the two small molecules, **TAT-TT** and **TAT-Cbz**, are shown in **Scheme 1.** Both molecules have been obtained from a cross-coupling reaction between two mono-brominated TAT units and a central chromophore. However, while the **TAT-TT** model has been synthesized through a Stille cross-coupling, using the 2-5-bis-trimethylstannyl-thieno[3,2-*b*]thiophene building block,[21]

the **TAT-Cbz** molecule has been synthesized through a Suzuki-Miyaura cross-coupling using the 2,7-bis(4,4,5,5-tetramethyl-1,3,2-dioxaborolan-2-yl)-9H-carbazole.
The new molecules exhibit high solubility in common organic solvents, such as tetrahydrofuran, chloroform, and methylene chloride. The purity and molecular structure were confirmed by NMR (see supporting information).

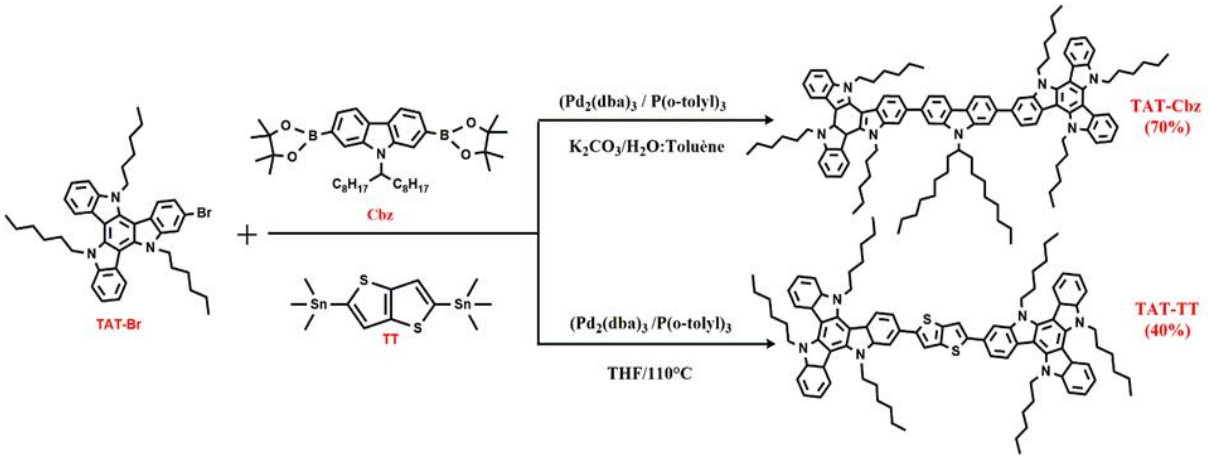

Scheme 1. Synthetic routes towards the two new dumbbell shaped small molecule.

Thermal properties of the new molecules were studied by thermogravimetric analysis (TGA) and differential scanning calorimetry (DSC) under inert nitrogen atmosphere. The thermograms are all shown in figure S7. Both molecules present high thermal stabilities with degradation temperatures above 400°C. No significant mass loss is noted before decomposition.
According to the DSC thermogram, the **TAT-TT** shows two endothermic peaks representative of melting transitions. The melting temperatures are respectively 69°C and 219°C. The first peak is associated to the glass transition at temperature (T_G), while the second transition corresponds to the molecular melting. **TAT-Cbz** exhibits a lower T_G at about 55°C followed by a melting temperature at 150°C. The observed shift in transition temperatures can be attributed to the presence of alkyl chains on the carbazole which provide fluidity.

3.2. Optoelectronic characterization and modeling

The electrochemical properties of **TAT-TT** and **TAT-Cbz** have been investigated by cyclic voltammetry (CV) in CH_2Cl_2 (DCM) (Figure 2). The potentials are given versus a saturated calomel electrode (SCE). The ionization potentials (IP or HOMO level) were calculated using the following formula: IP(eV) = E_{onset}^{ox} + 4.4. These formulas are based on the assumption that the energy level of SCE relative to vacuum is 4.4 eV as suggested by Jenekhe and coworkers.[22] Ferrocene was used as internal reference for calibration. As expected from the full electron donor nature of both molecules, they do not show any electroactivity in the anodic scan (absence of reduction waves, see Figure 2). On the other hand, the voltammograms display, in the cathodic region, several oxidation waves corresponding to the TAT and the central chromophores.[17]

For **TAT-TT**, the oxidation waves of TAT and TT overlap. In contrast, the oxidation waves of **TAT-Cbz** due to the different units are well defined. As expected, due to a stronger electron donor character, the Cbz unit leads to a positively shifted first oxidation wave as compared to the TT-counterpart. It results in a slightly deeper HOMO level, calculated at -4.8 eV for **TAT-Cbz** against -4.7 eV in **TAT-TT** molecule (Table 1). These values and the observed trend are in good agreement with the TD-DFT calculations (Table 1).

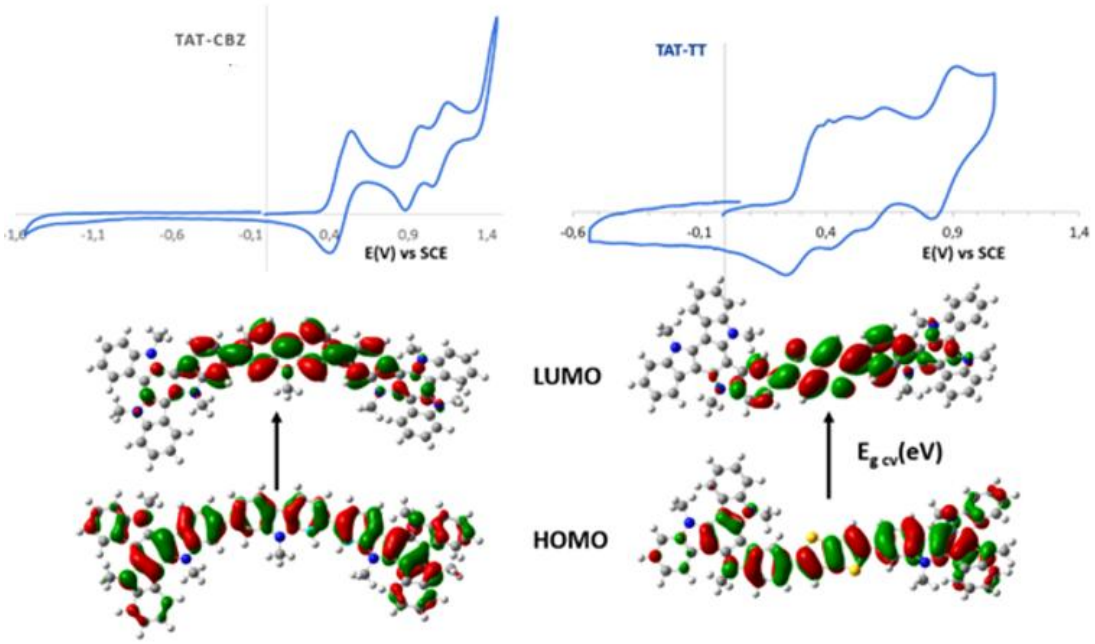

Figure 1. Top. Cyclic voltammograms of **TAT-Cbz** (left) and **TAT-TT** (right); scan rate: 150 mV.s^{-1}, platinum wire working electrode. Bottom. LUMO and HOMO boundary molecular orbitals using TD-DFT

UV–Visible absorption spectra were recorded at room temperature in DCM dilute solutions as well as in thin films. The absorption spectra are given in Figure 2 while the peak maxima of the energy transitions are reported in Table 1. The experimental data from solution are systematically compared with the theoretical values obtained by TD-DFT (CAM-B3LYP functional and 6-31G(d,p) using DCM as solvent), in order to validate and rationalize these values (see Table 1). More experimental details, including positions of observed absorption peaks, excitation energies, oscillator strengths (f), assignments of the principal excitation transitions, and electronic dipole moments are reported in Table S3.

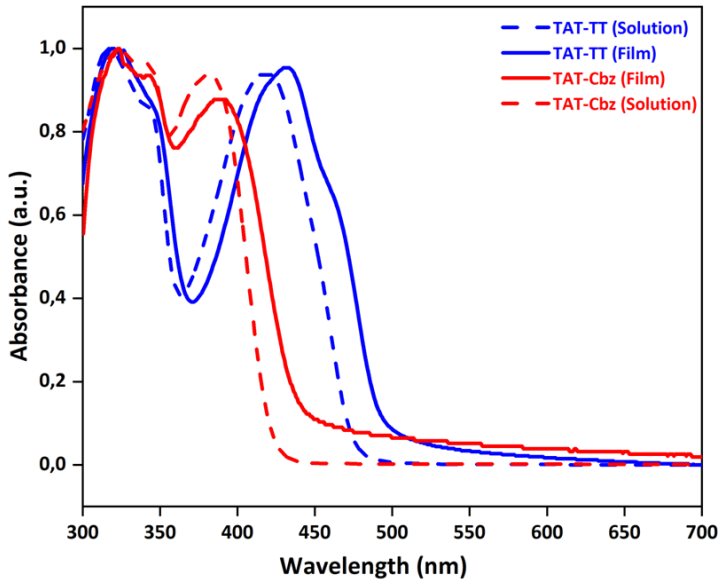

Figure 2. Absorption spectra in DCM solution (dashed line, concentration of 10^{-6} mol.L^{-1}) and in thin-films (full line) of **TAT-TT** (blue) and **TAT-Cbz** (red).

In solution, the absorption spectra of both molecules display two main bands (Figure 2). The first band is located in the deep UV region with a maximum at around 320 nm for both compounds, while the second band is red-shifted for **TAT-TT** with respect to **TAT-CBz**. **TAT-Cbz** absorbs only in the ultraviolet range (< 400 nm) with a maximum in solution located at 382 nm and an onset of absorption limited to 423 nm, while **TAT-TT** exhibits a maximum of absorption at 419 nm with an onset at 473 nm.

In order to validate and rationalize these experimental results, modeling has been carried out. First, a geometry optimization has been performed through the minimization of energy for both molecules by DFT (Table S1). Interestingly, both molecules exhibit different twisted geometries. Indeed, **TAT-TT** (Figure 3a) exhibits a geometry in which both dihedral angles between the TAT units and the central thienothiophene unit are identical and of about 25°, while **TAT-Cbz** has a more twisted structure with large dihedral angles of 144° (Figure 3a). The significantly higher torsion angle can be explained by the steric hindrance induced by both the alkyl side chain grafted on the carbazole unit as well as by the presence of aromatic protons on the benzene rings of neighboring TAT and carbazole units. In comparison, the lower cycle size of thiophene decreases the steric constraints on these positions and explains the higher conjugation seen on the absorption spectrum in solution for **TAT-TT**.

The calculated absorption spectra are in good agreement with the experimental ones and allow to ascribe the different bands to specific optical transitions (Figure 3b). Thus, for **TAT-TT**, the S0-S1 transition of energy 3.024 eV is attributed to a transition from the fully delocalized HOMO orbital to the LUMO level mainly localized on the TT and on the first neighboring indole groups. Concerning the higher energy band, although apparently different from the experimental measurement (one single band in the theoretical spectrum *vs* one band with a pronounced shoulder in the experimental spectrum), the calculated spectrum reveals two overlapping bands. The highest energy band is mainly attributed to a HOMO-2 to LUMO+1 transition, both located on only one single TAT unit, while the second band, which theoretically appeared as a shoulder due to a low oscillator strength, corresponds to a transition between the HOMO orbital and the LUMO+4 excited orbital, slightly delocalized over the whole molecule (Figure 3c).

Concerning the **TAT-Cbz** dye, the calculated spectrum shows a merging of the two experimentally observed bands. Actually, the highest energy band appears as a shoulder centered at 329 nm. It corresponds to a combination of several transitions from HOMO-1 and HOMO-3 orbitals towards excited LUMO+1 and LUMO+3 orbitals (Figure 3c). The second maximum at high wavelengths (369 nm) is attributed to an S0-S1 transition between the fully delocalized HOMO orbital to the LUMO, mainly delocalized over the central carbazole and the surrounding indole units, similarly to what has been seen in the **TAT-TT** molecule.

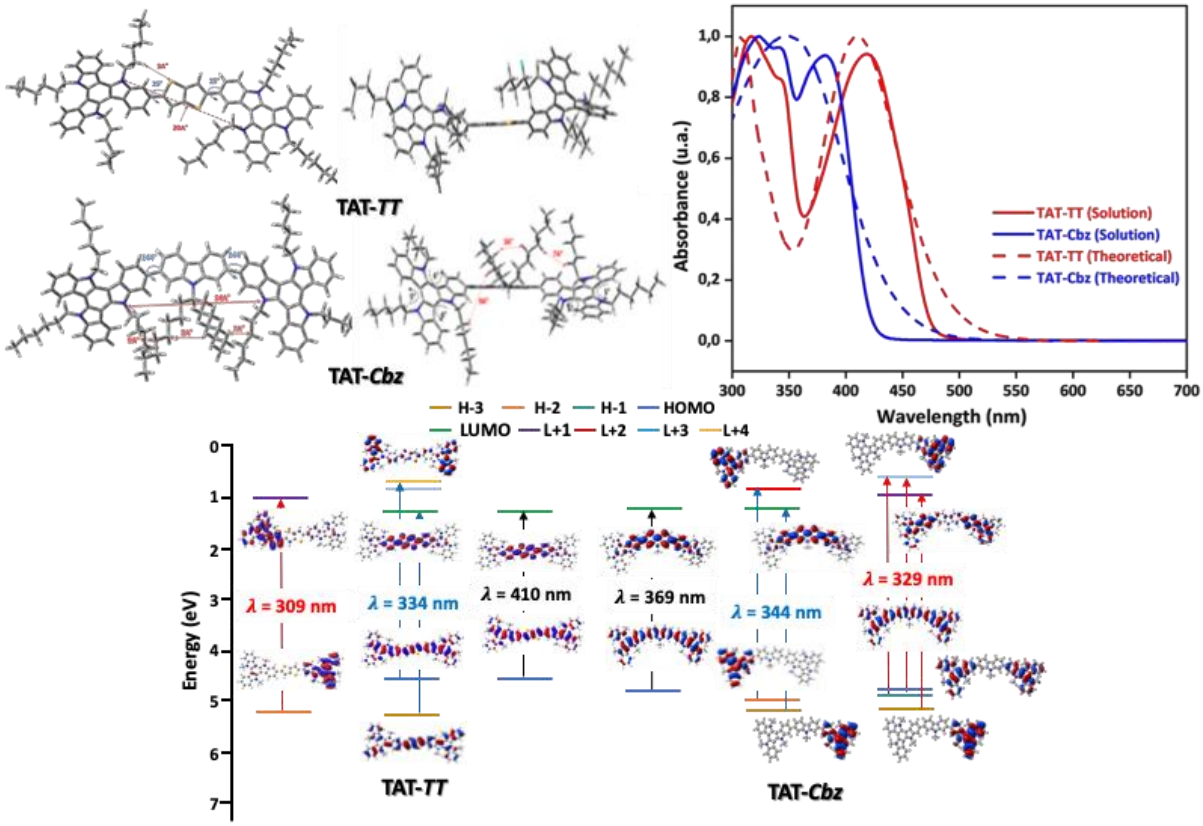

Figure 3. a) DFT/CAM-B3LYP/6-31G(d,p) optimized geometries for **TAT-TT** and **TAT-Cbz.** b) Comparison between experimental (full line) and theoretical (dashed line) absorption spectra of TAT-TT (red) and TAT-Cbz (blue). c) Distribution of the molecular orbitals of **TAT-TT** and **TAT-Cbz** obtained from TD-DFT calculations.

When going from solution to thin-films, the UV-Visible absorption spectra (Figure 2) of **TAT-TT** and **TAT-Cbz** undergo a slight bathochromic shift by roughly 20 and 12 nm, respectively. This redshift is generally attributed to π-π stacking interactions between neighboring molecules in the solid state The larger shift observed in **TAT-TT** in comparison to **TAT-Cbz** is in good agreement with the more planar **TAT-TT** geometry calculated by DFT. These bathochromic shifts lead to optical band-gaps of 2.51 eV and 2.81 eV for **TAT-TT** and **TAT-Cbz** dyes, respectively.

Table 1. Electrochemical and optical parameters of **TAT-TT** and **TAT-Cbz**.

	HOMO (eV)		λ_{max} [λ_{onset}] (nm)	ε_{max} (10^3 $M^{-1}.cm^{-1}$)	Eg_{-opt} (eV)
TAT-TT	- 4.67[a] (-4.58)[b]	Solution[c]	317; 342[d]; 419 [473]	228; 303	2.6
		Film	319; 346[d]; 432 [495]		2.5
TAT-Cbz	- 4.87[a] (-4.83)[b]	Solution[c]	324; 340[d]; 382 [423]	112; 106	2.9
		Film	322; 343[d]; 388 [441]		2.8

[(a)] Determined from cyclic voltammetry measurements in dichloromethane. [(b)] calculated experimentally. [(c)] DCM solution. [(d)] Shoulder

3.3. Charge transport and photovoltaic properties

To provide additional insight into these compounds, charge carrier mobilities have been determined by using them as the channel in bottom-gate/bottom contact (BG/BC) organic field-effect transistors (OFETs). The detailed elaboration and characterization procedure of devices can be found in the supporting information (see also Figures S8 and S9 for output characteristics). Hole mobility values

have been extracted from the saturation regime. As expected, the most planar **TAT-TT** molecule exhibits the highest hole mobility value, one decade higher than the **TAT-Cbz** counterpart (Table 2).

Table 2. Hole mobilities and OPV performances for **TAT-TT** and **TAT-Cbz**-based devices.

	μ_h (cm^2/V.s)	Voc (mV)	Jsc (mA/cm^2)	FF (%)	PCE (%)	AVT (%)
TAT-TT	(1.1 ± 0.2) x 10^{-4}	760	5.7	40.8	1.77	47.6
TAT-CBz	(1.5 ± 0.2) x 10^{-5}	860	0.4	36.0	0.12	86.4

Finally, the photovoltaic properties of these new TAT-based dumbbell-shaped molecules, as electron donor materials, have been investigated in solar cells using an inverted device configuration: ITO/PEIE/Active layer/MoO_3/Ag (details can be found in supplementary information). The $PC_{71}BM$ fullerene derivative has been selected to act as an electron acceptor material. After careful optimization, we found the best D:A ratio to be 1:3 for all molecules (Figure 4 and Table 2).
The **TAT-TT**:$PC_{71}BM$ bulk heterojunction (BHJ) leads to the best performance (Table 2), with a conversion efficiency of almost 1.8 % versus 0.1 % for the **TAT-Cbz**:$PC_{71}BM$ BHJ. The very low short circuit current density (Jsc) recorded in this latter is probably due to a combination of lower absorption and mobility. Both blends give reasonably high Voc. The highest Voc measured for the **TAT-Cbz** derivative is in good agreement with its deeper HOMO level. Obviously, both BHJ solar cells exhibit strong charge extraction problems with a current-density (J) under illumination that strongly increases (in absolute value) when the negative applied voltage increases. This is in-line with the low FF measured for both BHJs.

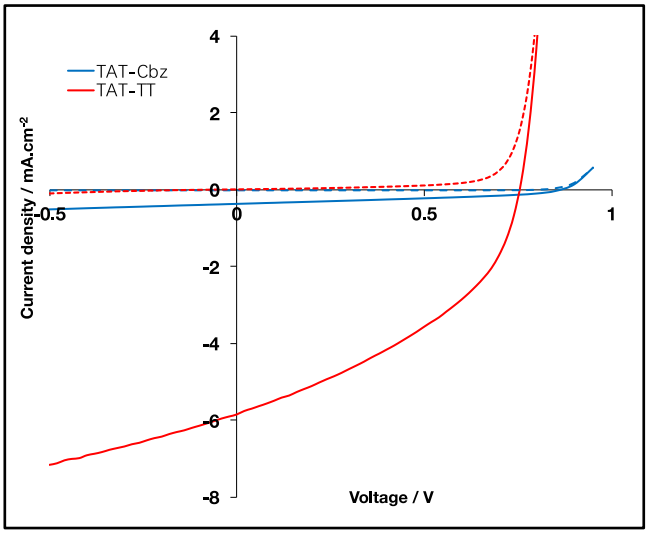

Figure 4. Measured J-V characteristics in a photovoltaic device using **TAT-TT** (red) and **TAT-Cbz** (blue) blended with $PC_{71}BM$. Dashed lines correspond to J-V characteristics under dark.

The average visible transmittance (AVT) can be estimated from the average transmittance of device active layer in the visible wavelength range of 400-700 nm (Figure 5).[23] The high AVT, above 86% measured for the **TAT-Cbz**, is offset by the very limited PCE. On the other hand, the 48% of AVT measured for the **TAT-TT** is very appealing, since it corresponds to a PCE close to 2%. Such a value is among the highest PCE reported for solution-processed semi-transparent solar cells exhibiting AVT close to 50%.

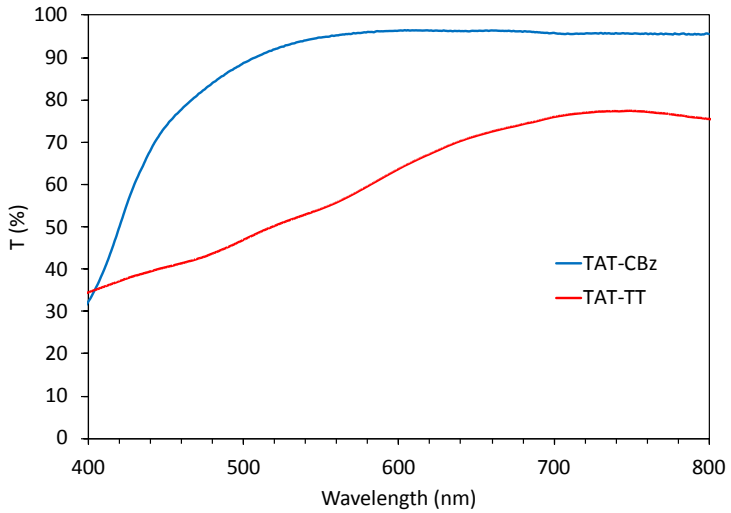

Figure 5. Transmission spectrum of the semi-transparent photovoltaic active layers based on the **TAT-Cbz** (blue) and on the **TAT-TT** (red).

4. Conclusion

In summary, we designed and synthesized two dumbbell-shaped small molecules including only electron donor units. These two molecules are found to exhibit high absorption, but limited to the near UV range, due to the reduced electronic conjugation. As each TAT fragment is carrying three alkyl side-chains, the molecules showed a remarkable solubility in a broad range of solvents. However, these side chains do not prevent a proper solid-state organization and both molecules have sufficient hole mobilities to be used in organic solar cells. Especially, the small size of the thieno[3,2-*b*]thiophene unit allows a good planarity of the conjugated backbone. Finally, used as near UV absorber in bulk heterojunction organic photovoltaic devices, the most conjugated **TAT-TT** derivative (including the thieno[3,2-*b*]thiophene moiety as a central chromophore), in blend with the $PC_{71}BM$ as electron-acceptor component, exhibits a 48% of average visible transmittance (AVT) with a PCE close to 2%. Such a value is among the highest PCE reported for solution-processed semi-transparent solar cells exhibiting AVT close to 50%.
This study constitutes one of the rare examples of solution-processable small molecules for transparent organic solar cells.

Acknowledgements

This work has been supported by the French National Research Agency (ANR PSLM project ANR-19-CE05-0036 contract).

Conflict of interest

The authors declare no conflict of interest.

Graphical abstract

Two new dumbbell-shaped small molecules are designed and investigated to be used as near ultra-violet absorbers for transparent organic solar cell application.

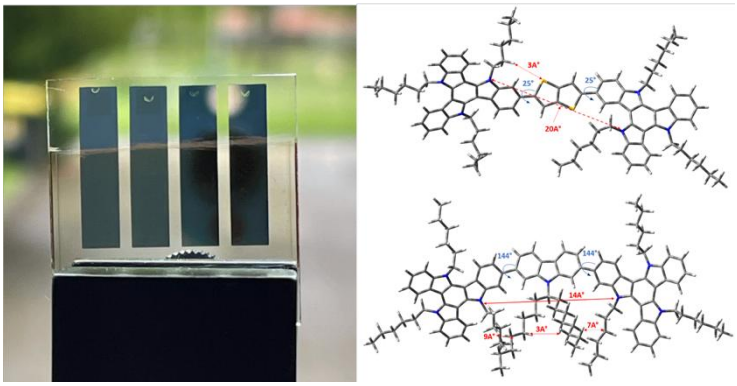

References

[1] Traverse CJ, Pandey R, Barr MC, Lunt RR. Emergence of highly transparent photovoltaics for distributed applications. Nat Energy 2017;2:849–60. https://doi.org/10.1038/s41560-017-0016-9.

[2] Lee K, Um H-D, Choi D, Park J, Kim N, Kim H, Seo K. The Development of Transparent Photovoltaics. Cell Reports Physical Science 2020;1:100143. https://doi.org/10.1016/j.xcrp.2020.100143.

[3] Anctil A, Lee E, Lunt RR. Net energy and cost benefit of transparent organic solar cells in building-integrated applications. Applied Energy 2020;261:114429. https://doi.org/10.1016/j.apenergy.2019.114429.

[4] Lee K, Kim N, Kim K, Um H-D, Jin W, Choi D, Park J, Lee S. Seo K. Neutral-Colored Transparent Crystalline Silicon Photovoltaics. Joule 2020;4:235–46. https://doi.org/10.1016/j.joule.2019.11.008.

[5] Hudson Baby B, Patel M, Lee K, Kim J, Large-Scale Transparent Photovoltaics for a Sustainable Energy Future: Review of Inorganic Transparent Photovoltaics. Appl. Sci. Converg. Technol. 2022;31 (1): 1-8. https://doi.org/10.5757/ASCT.2022.31.1.1.

[6] Chang S-Y, Cheng P, Li G, Yang Y. Transparent Polymer Photovoltaics for Solar Energy Harvesting and Beyond. Joule 2018;2:1039–54. https://doi.org/10.1016/j.joule.2018.04.005.

[7] Lee J, Cha H, Yao H, Hou J, Suh Y-H, Jeong S, Lee K, Durrant JR. Toward Visibly Transparent Organic Photovoltaic Cells Based on a Near-Infrared Harvesting Bulk Heterojunction Blend. ACS Appl Mater Interfaces 2020;12:32764–70. https://doi.org/10.1021/acsami.0c08037.

[8] Hu Z, Wang Z, An Q, Zhang F. Semitransparent polymer solar cells with 12.37% efficiency and 18.6% average visible transmittance. Science Bulletin 2020;65:131–7. https://doi.org/10.1016/j.scib.2019.09.016.

[9] Xie Y, Xia R, Li T, Ye L, Zhan X, Yip H, Sun Y. Highly Transparent Organic Solar Cells with All-Near-Infrared Photoactive Materials. Small Methods 2019;3:1900424. https://doi.org/10.1002/smtd.201900424.

[10] Davy NC, Sezen-Edmonds M, Gao J, Lin X, Liu A, Yao N, Kahn A, Loo Y-L. Pairing of near-ultraviolet solar cells with electrochromic windows for smart management of the solar spectrum. Nat Energy 2017;2:17104. https://doi.org/10.1038/nenergy.2017.104.

[11]Ullbrich S, Benduhn J, Jia X, Nikolis VC, Tvingstedt K, Piersimoni F, Roland S, Liu Y, Wu J, Fischer A, Neher D, Reineke S, Spoltore D, Wandewal K. Emissive and charge-generating donor–acceptor interfaces for organic optoelectronics with low voltage losses. Nat Mater 2019;18:459–64. https://doi.org/10.1038/s41563-019-0324-5.

[12] Jia X, Baird EC, Blochwitz-Nimoth J, Reineke S, Vandewal K, Spoltore D. Selectively absorbing small-molecule solar cells for self-powered electrochromic windows. Nano Energy 2021;89:106404. https://doi.org/10.1016/j.nanoen.2021.106404

[13] Bura T, Leclerc N, Bechara R, Lévêque P, Heiser T, Ziessel R. Triazatruxene-Diketopyrrolopyrrole Dumbbell-Shaped Molecules as Photoactive Electron Donor for High-Efficiency Solution Processed Organic Solar Cells. Adv Energy Mater 2013;3:1118–24. https://doi.org/10.1002/aenm.201300240.
[14] Bulut I, Lévêque P, Heinrich B, Heiser T, Bechara R, Zimmermann N, Méry S, Ziessel R, Leclerc N. LUMO's modulation by electron withdrawing unit modification in amorphous TAT dumbbell-shaped molecules. J Mater Chem A 2015;3:6620–8. https://doi.org/10.1039/C5TA00624D.
[15] Han T, Bulut I, Méry S, Heinrich B, Lévêque P, Leclerc N, Heiser T. Improved structural order by side-chain engineering of organic small molecules for photovoltaic applications. J Mater Chem C 2017;5:10794–800. https://doi.org/10.1039/C7TC03155F.
[16] Jing J, Heinrich B, Prel A, Steveler E, Han T, Bulut I, Méry S, Leroy Y, Leclerc N, Lévêque P, Rosenthal M, Ivanov DA, Heiser T. Efficient 3D charge transport in planar triazatruxene-based dumbbell-shaped molecules forming a bridged columnar phase. J Mater Chem A 2021;9:24315–24. https://doi.org/10.1039/D1TA06300F.
[17] Bulut I, Chávez P, Mirloup A, Huaulmé Q, Hébraud A, Heinrich B, Fall S, Méry S, Ziessel R, Heiser T, Lévêque P, Leclerc N. Thiazole-based scaffolding for high performance solar cells. J Mater Chem C 2016;4:4296–303. https://doi.org/10.1039/C6TC00531D.
[18] Bulut I, Huaulmé Q, Mirloup A, Chávez P, Fall S, Hébraud A, Méry S, Heinrich B, Heiser T, Lévêque P, Leclerc N. Rational Engineering of BODIPY-Bridged Trisindole Derivatives for Solar Cell Applications. ChemSusChem 2017;10:1878–82. https://doi.org/10.1002/cssc.201700465.
[19] Frisch A. Gaussian 09: users reference. Wallingford: Gaussian Inc.; 2009
[20] Dwivedi A, Kumar A. Molecular Docking and Comparative Vibrational Spectroscopic Analysis, HOMO-LUMO, Polarizabilities, and Hyperpolarizabilities of N -(4-Bromophenyl)-4-Nitrobenzamide by Different DFT (B3LYP, B3PW91, and MPW1PW91) Methods. Polycyclic Aromatic Compounds 2021;41:387–99. https://doi.org/10.1080/10406638.2019.1591466
[21] Biniek L, Chochos CL, Leclerc N, Hadziioannou G, Kallitsis JK, Bechara R, Lévêque P, Heiser T. A [3,2-b]thienothiophene-alt-benzothiadiazole copolymer for photovoltaic applications: design, synthesis, material characterization and device performances. J Mater Chem 2009;19:4946. https://doi.org/10.1039/b819177h.
[22] Kulkarni AP, Tonzola CJ, Babel A, Jenekhe SA. Electron Transport Materials for Organic Light-Emitting Diodes. Chem Mater 2004;16:4556–73. https://doi.org/10.1021/cm049473l.
[23] Shin D, Choi S-H. Recent Studies of Semitransparent Solar Cells. Coatings 2018;8:329. https://doi.org/10.3390/coatings8100329.